# Thermal–Hydraulic Analysis of a Model Coil for 40-T Hybrid Magnet Superconducting Outsert

Yong Ren, Yunfei Tan, Futang Wang, Wenge Chen, Jiawu Zhu, Junjie Li, Peng He, Zhiyou Chen, and Guangli Kuang

***Abstract*—A thermal–hydraulic performance analysis of a model coil for a 40-T hybrid magnet superconducting outsert being built at the High Magnetic Field Laboratory, Chinese Academy of Sciences, was performed. The model coil was wound with a $Nb_3Sn$ cable-in-conduit conductor cabled in a 316LN jacket cooled with supercritical helium. The model coil, in combination with 7.5-T NbTi solenoid coils, will be capable of generating a 12-T central field. Only one cooling channel was used to cool the model coil due to its short length. Both the temperature margin associated with a given scenario and the quench propagation following an artificial disturbance are discussed. The thermal–hydraulic analysis of the temperature margin showed that there is a sufficient minimum temperature margin for 100-A/s current ramp rate under a 7.5-T background magnetic field. The quench analysis showed that the hot-spot temperature of the cable is about 60 K, which is less than the maximum allowable value of 150 K for 0.7-s delay time. In addition, the convergence study was carried out for different time steps and space sizes.**

***Index Terms*—Cable-in-conduit conductor (CICC), model coil, superconducting magnet, thermal–hydraulic performance.**

## I. Introduction

The High Magnetic Field Laboratory of the Chinese Academy of Sciences is designing a 40-T hybrid magnet. The hybrid magnet consists of a 29-T resistive insert magnet and an 11-T superconducting outsert magnet [1]. The outsert consists of two parts, i.e., the inner one is a $Nb_3Sn$ coil made of a cable-in-conduit conductor (CICC) and the other one is a NbTi CICC coil. The layout of the $Nb_3Sn$ CICC conductor for the superconducting outsert is similar to that of the European Fusion Development Agreement dipole conductor with rectangular cross section and of the series-connected outsert at the National High Magnetic Field Laboratory [2]–[5]. The irreversible performance degradation of EFDA dipole conductor from cyclic transverse electromagnetic loads was observed in the past [2]. A $Nb_3Sn$ model coil, made of the same conductor as the superconducting outsert, was fabricated. On the one hand, the model coil was fabricated to gain the experience in the complicated fabrication process [6]–[10]. On the other hand, several test campaigns will be carried out to evaluate the performance degradation under the same electromagnetic load as the superconducting outsert. The main goals of the test campaigns were composed of quench propagation and thermal–hydraulic characteristics and the sensitivity of the current sharing temperature to cyclic operation. The model coil generates a central magnetic field of 4.5 T that operates at 16 500 A. The self-inductance and the corresponding stored energy of the model coil are 0.732 mH and 99.6 kJ, respectively. The model coil, in combination with NbTi solenoid coils generating a 7.5-T background central magnetic field, will provide a 12-T central magnetic field. The stored energy of the superconducting magnet system with 12-T central magnetic field is about 2.05 MJ. Table I lists the parameters of the model coil and of the 7.5-T background field coil. The 7.5-T solenoid coils, in combination with a water-cooled magnet, have been constructed as part of a 20-T hybrid magnet system 20 years ago. The 7.5-T solenoid coils will be updated as coils for generating a background magnetic field for the model coil [10], [11].

TABLE I
Main Parameters of the Two Superconducting Coils

| Coil name | | M1 | B1 | B2 |
|---|---|---|---|---|
| Strand | | $Nb_3Sn$/Cu | NbTi | |
| Inner diameter | mm | 120.4 | 336.0 | 393.0 |
| Outer diameter | mm | 226.0 | 393.0 | 480.3 |
| Length | mm | 529.2 | 552.0 | 552.0 |
| Layer | | 6 | 14 | 24 |
| Total turns | | 126 | 1890 | 3792 |
| Void fraction | | 0.29±0.01 | | |
| No. of $Nb_3Sn$ strands | | 128 | | |
| No. of Cu strands | | 64 | | |
| Operating current | A | 16500 | 725 | |
| Stored energy | MJ | 2.05 | | |
| Central magnetic field | T | 12.14 | | |

In the past, several codes were used to analyze the thermal–hydraulic behavior of superconducting coils made of CICC using 1-D or multidimensional model [12]–[17]. More accurate results could be obtained with multidimensional code by considering the interturn and interlayer heat transfer compared with the 1-D code (e.g., Gandalf code). However, Gandalf and a quasi 3-D code (e.g., Vincenta) are overall giving the same results apart from acceptable differences [14], [18]. Here, 1-D GANDALF code was used to analyze the thermal–hydraulic performance of the model coil. On the one hand, the input file can be easily modified through an external subroutine. On the other hand, the adaptive mesh technique can be used in case of quench [12]. In this paper, the minimum temperature margin to cyclic operation for a ramp rate of 100 A/s and quench propagation following an artificial disturbance were analyzed by modifying the magnetic field, strain, power losses, variable with time along the cooling path, and friction factor of the CICC through external subroutines.

## II. Description of the Model Coil and the Relevant Input Parameters

The model coil consists of 126 turns with a total length of about 80 m. All turns have the same CICC configuration. The CICC conductor with rectangular cross section consists of 192 strands with 128 $Nb_3Sn$ strands and 64 copper strands, each with a diameter of 0.81 mm. The cables were wrapped with stainless steel tape to reduce surface damage of the strands during the manufacturing process. Fig. 1 shows the cross section of the CICC conductor after heat treatment. The conductor hydraulic data are listed in Table II. Only one cooling channel was adopted to cool the whole winding due to its short length. The model coil was cooled with forced flow helium at 4.7 K and 5 bar at the inlet. The steady-state mass flow rate adopted was 1 g/s. The relevant input parameters used for the thermal–hydraulic analysis of the model coil for the 40-T hybrid magnet superconducting outsert are described below.

### A. Superconducting Strand Scaling Law

The $Nb_3Sn$ strands adopted were restack rod process internal-tin-type strands with high critical current density $\sim$2200 A/mm$^2$ at 4.2 K and 12 T. The critical current of the $Nb_3Sn$ strand with 0.8-mm diameter selected is calculated using the Twente scaling law,

Manuscript received March 26, 2011; revised September 11, 2011; accepted November 24, 2011. Date of current version March 30, 2012. This work was supported in part by the National Development and Reform Commission of China and in part by the Chinese Academy of Sciences. This paper was recommended by Associate Editor A. Devred.

The authors are with the High Magnetic Field Laboratory, Chinese Academy of Sciences, Hefei 230031, China (e-mail: renyong@mail.ustc.edu.cn; kuang_gl@ipp.ac.cn).

Color versions of one or more of the figures in this paper are available online at http://ieeexplore.ieee.org.

Digital Object Identifier 10.1109/TASC.2011.2178069

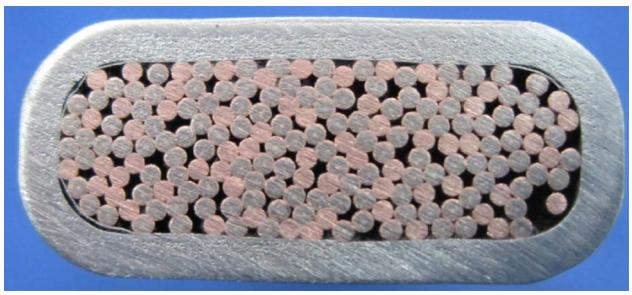

Fig. 1. Cross section of the CICC conductor after heat treatment.

TABLE II
PARAMETERS OF THE CICC

| | | | |
|---|---|---|---|
| Length | L | m | 80 |
| $Nb_3Sn$ cross section | $A_{SC}$ | $mm^2$ | 33.6 |
| Copper cross section | $A_{Cu}$ | $mm^2$ | 67.2 |
| Helium cross section | $A_{He}$ | $mm^2$ | 41.2 |
| SS jaket cross section | $A_{SS}$ | $mm^2$ | 97.6 |
| Jacket thickness | | mm | 1.6 |
| Void fraction | $V_f$ | - | 0.29 |
| RRR | | - | 100 |
| Conductor helium wetted perimeter | PHTC | m | 0.415 |
| Jacket helium wetted perimeter | PHTJ | m | 0.0313 |
| Jacket conductor wetted perimeter | PHTCJ | m | 0.0313 |
| Hydraulic diameter | $D_h$ | mm | 0.369 |

TABLE III
STRAND CHARACTERIZATION PARAMETERS OF THE MODEL COIL

| Parameter | value | |
|---|---|---|
| Ca1 | 38.51 | |
| Ca2 | 0.0 | |
| Eps_0a | 0.401% | |
| Eps_m | -0.160% | |
| Bc2m(0) | 28.27 | T |
| Tcm | 16.25 | K |
| C | 47476 | A*T |
| P | 0.53 | - |
| Q | 1.92 | - |

as described in [19] in [20]. The effective filament diameter of the strand adopted for the ac loss calculation was 80 $\mu$m, according to the measured results of a single strand. Table III gives the strand characterization parameters of the model coil.

### B. Fiction Factor of the CICC

The friction factors are derived from the measurements [21], and the pressure drop per unit length along the flow direction can be described as follows:

$$\frac{\partial p}{\partial x} = -2\rho \frac{f}{D_h} v\,|v| \tag{1}$$

where $p$ is the pressure, $\rho$ is the density, $f$ is the friction factor, $v$ is the flow velocity, $D_h = 4\,\mathrm{A_{He}}/P_w$ is the hydraulic diameter of the CICC, $A_{\mathrm{He}}$ is the cross section of the fluid, $P_w = 5/6\pi N_{\mathrm{st}} d_{\mathrm{st}} + 0.5 P_{\mathrm{jk}}$ is the wetted perimeter, $N_{\mathrm{st}}$ is the number of strands, $d_{\mathrm{st}}$ is the strand diameter, and $P_{\mathrm{jk}}$ is the inner perimeter of the jacket.

The friction factor of the CICC can be characterized by Katheder correlation [22], which can be described as follows [21]:

$$f = 0.25 \frac{1}{v_f^{0.897}} \left(0.0237 + \frac{19.5}{\mathrm{Re}^{0.954}}\right) \tag{2}$$

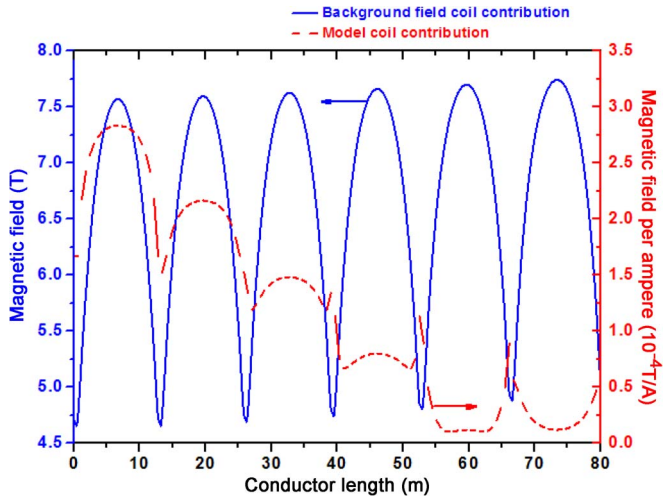


Fig. 2. Magnetic field distribution along the cooling length generated by background field and model coils.

where $v_f$ is the void fraction, and Re is the Reynolds number, which can be defined as

$$\mathrm{Re} = \frac{\rho v D_h}{\mu} \tag{3}$$

where $\mu$ is the viscosity.

As described in many papers [23], [24], a large relative error could be obtained between the friction factor characterized by Katheder correlation and the experimental results. The relative error between formula (2) and the experimental results is within $\pm 20\%$. Therefore, a multiplier of 1.2 as a safety factor is selected, which would allow a conservative prediction of the thermal–hydraulic behavior of the CICC.

### C. Heat Sources

The heat sources mainly consist of two parts, i.e., ac losses, which consist of hysteresis loss and coupling loss, and resistive heating generated by superconducting joint with 3 n$\Omega$ of 0.3-m length. The accurate evaluation of the coupling loss of the CICC conductor is a hard work because there are no data available of the time constant for the model coil before testing it. The time constant of $Nb_3Sn$ CICC conductor is affected by its void fraction, cable pattern, aspect ratio, coating material, applied load, load history, and the magnet ramp rate, etc. [25]–[30]. For simplicity, time constants $n$ and $\tau$ were selected as 175 and 40 ms for magnet ramp and magnet quench, respectively [31]. In our analysis, only inlet joint heating is included.

## III. MINIMUM TEMPERATURE MARGIN ANALYSIS FOR CONTINUOUS CYCLING OPERATION

In order to evaluate the current sharing temperature sensitivity of the model coil to cyclic transverse electromagnetic loads, several cycle tests are required. Therefore, the prediction of the minimum temperature margin of the model coil to a given ramping rate during cyclic operation is required. Fig. 2 shows the central magnetic field generated by background field coil and the magnetic field per ampere generated by the model coil. The operation of the magnet system is as follows. First, the background field coil was ramped up to the rated magnetic field of 7.5 T for about 20 min. The heat deposition on the model coil generated by the changed magnetic field was removed with forced flow helium during this period. Therefore, we assume that the initial

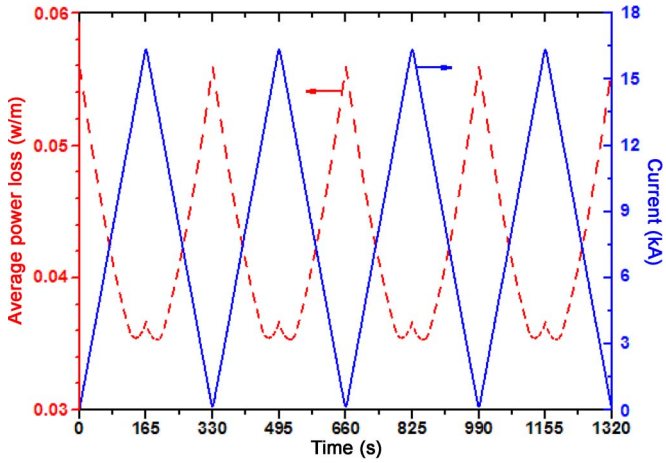


Fig. 3. Dependence of average power loss and current as a function of time.

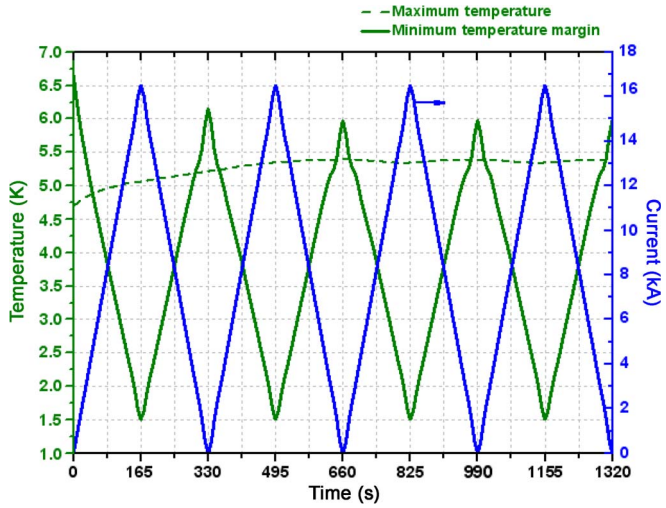


Fig. 4. Maximum temperature and minimum temperature margins of the cable during continuous cyclic operation at 100-A/s ramp rate along the cooling length of the model coil.

temperature along the entire cooling channel of the model coil was the setting value of 4.7 K. The inlet and outlet pressures are 5 and 4.38 bar, respectively, which will cause the steady-state flow rate of 1 g/s. For conservative, we assume that the $Nb_3Sn$ superconductor has an 80% carrying current capacity and the thermal strain is $-0.75\%$. In addition, degradation of the model coil was not considered for ac loss calculation. Fig. 3 shows the dependence of the current and power loss, including ac loss and joint heating as a function of time. Fig. 4 gives the maximum temperature and minimum temperature margins of the cable during continuous cyclic operation at 100-A/s ramp rate along the cooling channel of the model coil. The minimum temperature margin of the cable was located in the middle of the innermost layer where the magnetic field is highest when the model coil is ramped up the full field. The cable maximum temperature is less than 5.5 K. The minimum temperature margin is about 1.5 K, which is larger than the designed value of 1 K. Fig. 5 shows the outlet temperature of the model coil as a function of time during continuous cyclic operation at 100 A/s.

The minimum temperature margin is a key parameter for the operation of the model coil. The hysteresis loss plays an important role at lower current ramp rate (e.g., $dI/dt < 100$ A/s in this case). In fact, the ramp rate of the model coil is far less than the value of 100 A/s to cyclic operation during a test. In addition, heat generated by ac

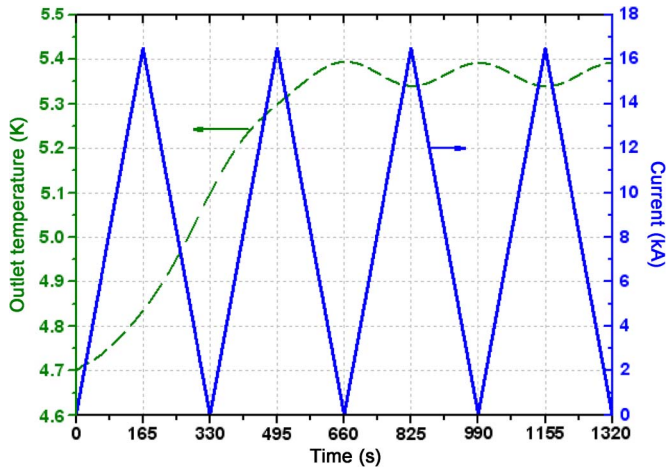


Fig. 5. Outlet temperature of the model coil as a function of time during continuous cyclic operation at 100-A/s ramp rate.

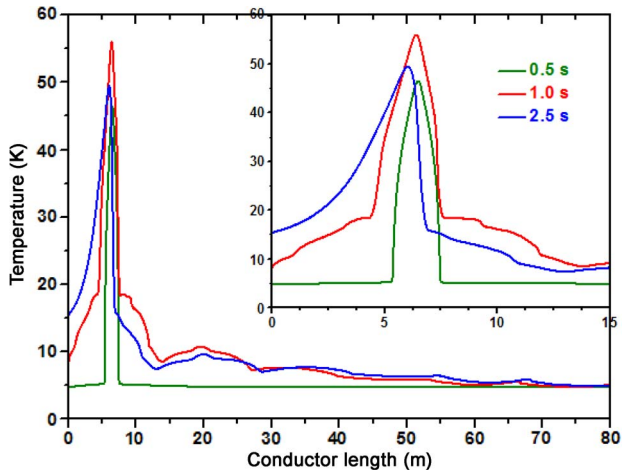


Fig. 6. Temperature profile along the conductor length.

losses and joint heating can be quickly evacuated from the location of the magnetic field peak value. The minimum temperature does not significantly change for several current ramp rates ($<$ 100 A/s) because the maximum magnetic field location does not coincide the temperature peaks along the cooling length. The minimum temperature margin is strongly affected by the thermal strain from heat treatment temperature to operating temperature. The analysis results show that the minimum temperature margins for assuming thermal strain of $-0.75\%$, $-0.70\%$, and $-0.65\%$ are 1.5 K, 1.78 K, and 2.04 K when the model coil is ramped up to the full field, respectively. In fact, the critical current density of the $Nb_3Sn$ superconductor is more sensitive to strain effects than that of the ac losses in this case.

## IV. Quench Analysis

From the point of view of quench protection of the model coil, it is vital to analyze the hot-spot temperature of a cable and the maximum helium pressure in a stainless steel conduit during a quench unexpected. To initiate a quench, a square heat pulse with duration/length (0.03 s, 0.1 m) assumed was introduced in the middle of the innermost layer of the model coil for simulating an unexpected disturbance. The magnetic field variation with time along the cooling channel length is considered for the quench analysis. The initial current, operating temperature, and mass flow rate were 16 500 A, 4.7 K, and 1 g/s, respectively. The model coil is connected with the constant pressure reservoirs at inlet and outlet. During a quench, the boundary of the inlet

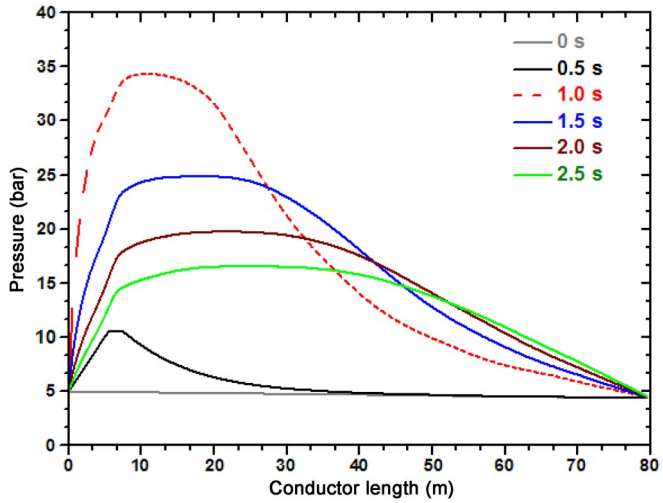


Fig. 7. Pressure profile along the conductor length.

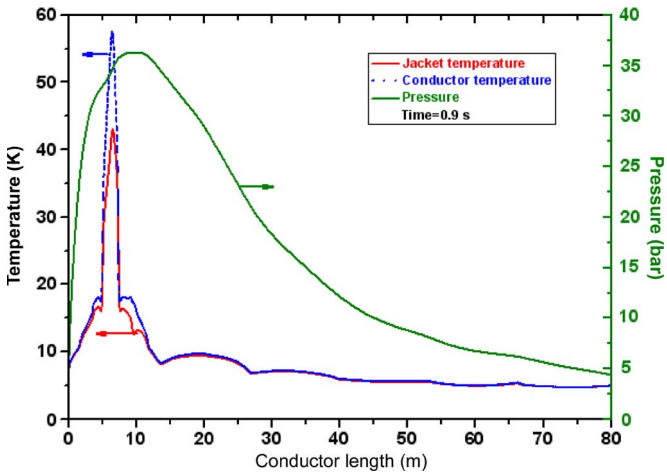


Fig. 8. Cable and jacket temperatures and helium pressure in a jacket distribution along the cooling channel at 0.9 s during a quench.

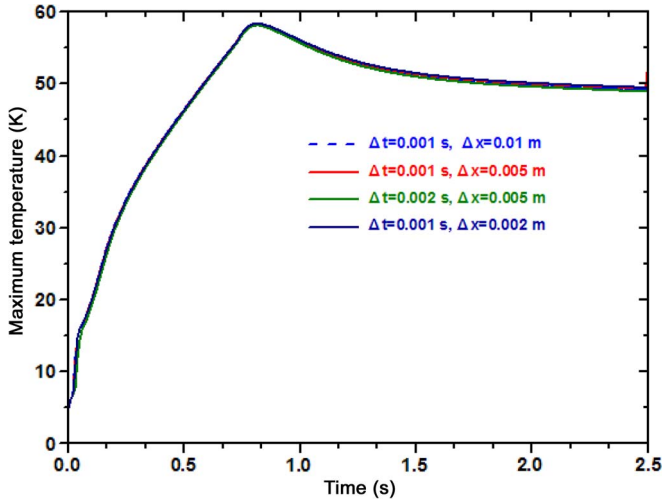


Fig. 9. Maximum temperature as a function of time for different time steps and space sizes during a quench.

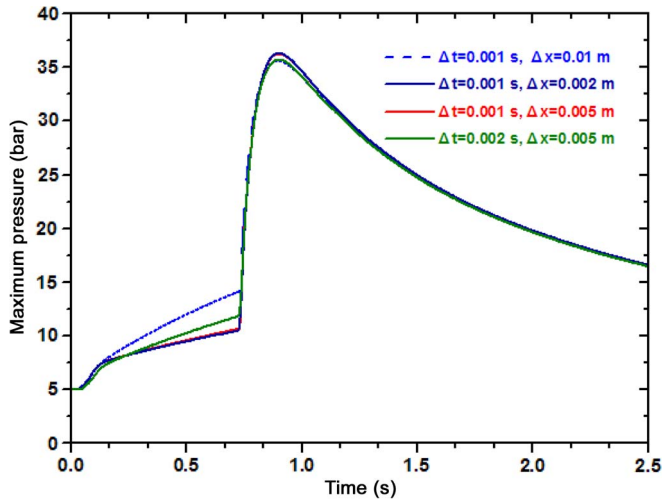


Fig. 10. Maximum pressure as a function of time for different time steps and space sizes during a quench.

and the outlet is complicated due to the coupling between the model coil and its external cryogenic circuit. The fixed boundary condition for the inlet and outlet pressures is exerted, but the temperature is changing in the analysis.

The following quench performance analysis is based on the selection of delay time $t = 0.7$ s. The dump resistor $R_1$ of the model coil was selected as 3.6 m$\Omega$. The exponential decay of time period is about 0.2 s. The current rapidly decreases after opening of the breaker. Fig. 6 shows the temperature profile with quench times $t = 0.5, 1,$ and 2.5 s along the cooling length. The hot-spot temperature was less than 60 K at 1 s. Fig. 7 shows the pressure profile in a stainless steel jacket with quench times of 0.5, 1, 1.5, 2, and 2.5 s along the cooling length. The maximum helium pressure was about 35 bars at 1 s. Fig. 8 shows the distribution of cable and jacket temperatures and of the helium pressure in the jacket along the cooling channel at 0.9 s during a quench. The maximum temperature of the jacket is about 43 K, whereas the maximum temperature of the cable is about 57 K. The latter temperature is less than the maximum permissible temperature of 150 K. The maximum pressure in the 316LN stainless steel jacket is about 36 bars. The larger helium pressure in the 316LN jacket can reduce the stress of the conduit to some degree [32]. However, the 316LN stainless steel strength will be reduced with the increased jacket temperature [33]. The analysis showed that the stress of the jacket is within the allowable value.

The numerical convergence of the quench simulation is of great importance from the point of view of accuracy of the analysis. Generally, the simulation results independent of the time step and space mesh densities are required for quench study. Figs. 9 and 10 give the results on maximum pressure and maximum temperature evolution for different time steps and space mesh sizes. For quench simulation aforementioned, as shown in Figs. 6–8, a time step of 0.001 s and a space size of 0.005 m are adopted.

## V. Conclusion

The detailed thermal–hydraulic analysis of a model coil for a 40-T hybrid magnet superconducting outsert magnet using a 1-D software GANDALF code has been performed. The temperature margin analysis showed that there is an adequate minimum temperature margin during cyclic operation for a current ramp rate of 100 A/s. The minimum temperature margin of the $Nb_3Sn$ CICC conductor is more sensitive to strain effects than that of the ac losses in this case. The quench analysis showed that the hot-spot temperature of the model coil is about 60 K for delay time of 0.7 s, which is less than the maximum allowable temperature of 150 K. The model coil can be safely protected with the protection mode without damaging during a quench. The accuracy of the analysis is obtained by suitable convergence

studies with different time steps and space sizes for quench propagation. In addition, as a further study, we will resort to a 3-D model to analyze the thermal–hydraulic behavior of the model coil.

## REFERENCES


[1] Y. F. Tan, F. T. Wang, Z. M. Chen, Y. N. Pan, and G. L. Kuang, "The design of cable-in-conduit conductors for the superconducting outsert coils of a 40 T hybrid magnet," *Supercond. Sci. Technol.*, vol. 22, no. 2, p. 025 010, Feb. 2009.

[2] A. Voster, P. Bauer, R. Wesche, U. Besi Vetrella, B. Stepanov, A. della Corte, A. Portone, E. Salpietro, and P. Bruzzone, "Development of the EFDA dipole high field conductor," *IEEE Trans. Appl. Supercond.*, vol. 18, no. 2, pp. 544–547, Jun. 2008.

[3] I. R. Dixon, M. D. Bird, P. Bruzzone, A. V. Gavrilin, J. Lu, B. Stepanov, and H. W. Weijers, "Current sharing and AC loss measurements of a cable-in-conduit conductor with $Nb_3Sn$ strands for the high field section of the Series-Connected Hybrid outsert coil," *IEEE Trans. Appl. Supercond.*, vol. 19, no. 3, pp. 2466–2469, Jun. 2009.

[4] I. R. Dixon, M. D. Bird, K. R. Cantrell, J. Lu, R. P. Walsh, and H. W. Weijers, "Qualification measurements of the mid-field and low-field CICC for the series-connected hybrid magnet with effects of electromagnetic load cycling and longitudinal strain," *IEEE Trans. Appl. Supercond.*, vol. 20, no. 3, pp. 1459–1462, Jun. 2010.

[5] P. Bruzzone, B. Stepanov, R. Wesche, A. Portone, E. Salpietro, A. Vostner, and A. della Corte, "Test results of a small size CICC with advanced $Nb_3Sn$ strands," *IEEE Trans. Appl. Supercond.*, vol. 16, no. 2, pp. 894–897, Jun. 2006.

[6] Y. F. Tan, W. Chen, Y. Pan, F. Wang, Z. Chen, J. Zhu, and G. Kuang, "A conceptual design of model coil for the 40 T hybrid magnet superconducting outsert," *IEEE Trans. Appl. Supercond.*, vol. 19, no. 6, pp. 3790–3794, Dec. 2009.

[7] W. G. Chen, Z. M. Chen, Y. N. Pan, F. T. Wang, Z. Y. Chen, Y. F. Tan, J. W. Zhu, Y. Ren, P. He, and G. L. Kuang, "Engineering design of the superconducting outsert for 40 T hybrid magnet," *IEEE Trans. Appl. Supercond.*, vol. 20, no. 3, pp. 1920–1923, Jun. 2010.

[8] G. Kuang, "A 40 T hybrid magnet under construction in China," *IEEE Trans. Appl. Supercond.*, vol. 20, no. 3, pp. 680–683, Jun. 2010.

[9] J. W. Zhu, Y. N. Pan, W. G. Chen, Y. F. Tan, F. T. Wang, Z. M. Chen, Z. Y. Chen, P. He, Y. Ren, and G. L. Kuang, "Mechanical behavior analysis of model coil for the 40-T hybrid magnet superconducting outsert," *IEEE Trans. Appl. Supercond.*, vol. 20, no. 3, pp. 628–631, May 2010.

[10] Y. Ren, "Magnetic force calculation between misaligned coils for a superconducting magnet," *IEEE Trans. Appl. Supercond.*, vol. 20, no. 6, pp. 2350–2353, Dec. 2010.

[11] F. T. Wang, J. L. Chen, H. M. Han, Z. Huang, Y. F. Bi, Z. K. Jiao, and B. J. Gao, "Development and tests results of the superconducting coil of the hybrid magnet," *Chin. J. Low Temp. Phys.*, vol. 13, no. 3, pp. 239–244, May 1991.

[12] L. Bottura, "A numerical model for the simulation of quench in the ITER magnets," *J. Comput. Phys.*, vol. 125, no. 1, pp. 26–41, Apr. 1996.

[13] R. Zanino, D. Bessette, and L. Savoldi Richard, "Quench analysis of an ITER TF coil," *Fusion Eng. Des.*, vol. 85, no. 5, pp. 752–760, Aug. 2010.

[14] C. Meuris, S. Nicollet, and W. Abdel Maksoud, "Using the Vincenta code to analyse pressure increase in helium during the quench of a superconducting magnet," *Cryogenics*, vol. 50, no. 3, pp. 177–186, Mar. 2010.

[15] R. Zanino, N. Mitchell, and L. Savoldi Richard, "Analysis and interpretation of the full set (2000–2002) of Tcs tests in conductor 1A of the ITER central solenoid model coil," *Cryogenics*, vol. 43, pp. 752–760, 2010.

[16] Q. Wang, P. Weng, and M. He, "Simulation of quench for the cable-in-conduit conductor in HT-7U superconducting Tokamak magnets using porous medium model," *Cryogenics*, vol. 44, no. 2, pp. 81–92, Feb. 2004.

[17] R. Zanino, R. Bonifetto, R. Heller, and L. S. Richard, "Validation of the 4C thermal–hydraulic code against 25 kA safety discharge in the ITER toroidal field model coil (TFMC)," *IEEE Trans. Appl. Supercond.*, vol. 21, no. 3, pp. 1948–1952, Jun. 2011.

[18] S. Nicollet, D. Bessette, D. Ciazynski, J. L. Duchateau, and B. Lacroix, "Cross checking of Gandalf and Vincenta on the CS behaviour during ITER reference scenario," in *Proc. Adv. Cryogenic Eng.*, 2010, pp. 1402–1409.

[19] Y. F. Tan, W. Chen, Z. Chen, P. He, J. Zhu, Y. Ren, Y. Pan, F. Wang, Z. Chen, and G. Kuang, "Characterization of $Nb_3Sn$ strands for a 40-T hybrid magnetic model coil," *IEEE Trans. Appl. Supercond.*, vol. 21, no. 4, pp. 3447–3451, Aug. 2010.

[20] A. Godeke, B. ten Haken, H. H. J. ten Kate, and D. C. Larbalestier, "A general scaling relation for the critical current density in $Nb_3Sn$ conceptual design of model coil for the 40 T hybrid magnet superconducting outsert," *Supercond. Sci. Technol.*, vol. 19, no. 6, pp. R100–R116, 2006.

[21] J. Li, Z. Ouyang, and L. Shi, "Friction factor measurements on CICC for 40-T hybrid superconducting outsert," *Cryo. Supercond.*, vol. 39, no. 1, pp. 22–24, Jun. 2011.

[22] H. Katheder, "Optimum thermalhydraulic operation regime for cable in conduit, superconductors (CICs)," *Cryogenics*, vol. 34, pp. 595–598, 1994.

[23] R. Zanino and L. Savoldi Richard, "A review of thermal–hydraulic issues in ITER cable-in-conduit conductors," *Cryogenics*, vol. 46, no. 7/8, pp. 541–555, Jul./Aug. 2006.

[24] M. Bagnasco, L. Bottura, and M. Lewandowska, "Friction factor correlation for CICC's based on a porous media analogy," *Cryogenics*, vol. 50, no. 11/12, pp. 711–719, Nov./Dec. 2010.

[25] P. Bruzzone, B. Stepanov, and E. Zapretilina, "A critical review of coupling loss results for cable-in-conduit conductors," *IEEE Trans. Appl. Supercond.*, vol. 16, no. 2, pp. 827–830, Jun. 2006.

[26] P. Bruzzone, B. Stepanov, R. Wesche, A. della Corte, L. Affinito, M. Napolitano, and A. Vostner, "Test results of a $Nb_3Sn$ cable-in-conduit conductor with variable pitch sequence," *IEEE Trans. Appl. Supercond.*, vol. 19, no. 3, pp. 1448–1451, Jun. 2009.

[27] K. Hamada, Y. Takahashi, K. Matsui, T. Kato, and K. Okuno, "Effect of electromagnetic force on the pressure drop and coupling loss of a cable-in-conduit conductor," *Cryogenics*, vol. 44, no. 1, pp. 45–52, Jan. 2004.

[28] Y. A. Ilyin, D. Bessette, E. Zapretilina, C. Luongo, F. Simon, B. S. Lim, and N. Mitchell, "Performance analysis of the ITER poloidal field coil conductors," *IEEE Trans. Appl. Supercond.*, vol. 20, no. 3, pp. 415–418, Jun. 2010.

[29] F. Cau and P. Bruzzone, "Dependence of the AC loss on the aspect ratio in a cable in conduit conductor," *Supercond. Sci. Technol.*, vol. 23, no. 4, p. 045 011, Apr. 2010.

[30] F. Cau and P. Bruzzone, "AC loss measurements in CICC with different aspect ratio," *IEEE Trans. Appl. Supercond.*, vol. 19, no. 3, pp. 2383–2386, Jun. 2009.

[31] J. Lu, "SCH CICC test results and interpretation," SCH Design Review, NHMFL2009, Jan..

[32] I. R. Dixon, M. D. Bird, and J. R. Miller, "Mechanical design of the series connected hybrid magnet superconducting outsert," *IEEE Trans. Appl. Supercond.*, vol. 16, no. 2, pp. 981–984, Jun. 2006.

[33] Y. Zhai, I. R. Dixon, and M. D. Bird, "Mechanical analysis of the superconducting outsert for the series connected hybrid magnets," *IEEE Trans. Appl. Supercond.*, vol. 19, no. 3, pp. 1608–1611, Jun. 2009.